

# Journal of Mechanics of Materials and Structures

**AXISYMMETRIC LOADING OF AN ELASTIC-PLASTIC PLATE  
ON A GENERAL TWO-PARAMETER FOUNDATION**

Luca Lanzoni, Andrea Nobili, Enrico Radi and Andrea Sorzia

**Volume 10, No. 4**

**July 2015**





## AXISYMMETRIC LOADING OF AN ELASTIC-PLASTIC PLATE ON A GENERAL TWO-PARAMETER FOUNDATION

LUCA LANZONI, ANDREA NOBILI, ENRICO RADI AND ANDREA SORZIA

The load carrying capacity and collapse scenarios for an infinite elastic-plastic plate resting on a two-parameter elastic foundation uniformly loaded on a small circular footprint are investigated in a general framework of stiffness and yield parameters. The present work extends the study already presented for a specific value of the Pasternak modulus and it allows the investigation of the influence of the stiffness property of the underlying soil and the amplitude of the loaded region on the load carrying capacity of the plate and the corresponding collapse mechanism. Moreover, the present analysis allows for the evaluation of the transverse deflection, slope, radial and circumferential bending moments, shearing force within the plate and the reactive pressure of the elastic subgrade at the onset of the plastic collapse together with their dependence on the foundation moduli. The effect of the ratio between negative and positive yield moments is also investigated. The amplitude and assembly of plastic regions at the onset of the plastic collapse are discussed in some detail.

### 1. Introduction

The problem of a plate resting on an elastic subgrade has been extensively investigated in the literature because of its relevance in many structural and geotechnical applications. Indeed, plate and slab-like elements supported by an elastic foundation are commonly encountered in many engineering systems, with particular reference to design spread building foundations (particularly, shallow mat-like foundations), e.g., [Gazetas and Tassios 1978; Gazetas 1981a], industrial and airport pavements [Caliendo and Parisi 2010], and rigid or flexible roadways [Helwany et al. 1998].

According to its relative slenderness, a shallow building foundation can be modeled as a thin Kirchhoff plate or as a thick Reissner–Mindlin plate, whereas the supporting medium can be simulated in different ways. As is well known, the perhaps most popular foundation model was proposed by Winkler in 1867, and it has enjoyed wide popularity ever since on account of its greater simplicity with respect to other soil descriptions at a reasonable cost in terms of result reliance in the supported structure. Nonetheless, owing to its local nature, the Winkler model cannot produce accurate results for the displacement field of the soil-foundation system. Accordingly, a variety of nonlocal subgrade models (e.g., Pasternak, Reissner, Filonenko-Borodich, Hetényi, Kerr and Vlazov models, among others) has been proposed over the years to improve upon the Winkler-type soil model [Selvadurai 1979].

Several analytical and numerical studies have been performed to evaluate the mechanical interaction between a raft slab foundation and the supporting medium. The analytical solution of a thin Kirchhoff plate resting on a Winkler-type subgrade under various load conditions is reported in detail in the classical

---

*Keywords:* two-parameter subgrade, Kirchhoff plate, Johansen's yield criterion, axisymmetric loading conditions, contour integral, elastic-plastic collapse.

book of Timoshenko and Woinowsky-Krieger [1959]. The axisymmetric flexure of an infinite elastic plate resting on an incompressible elastic half-space is considered by Selvadurai [1977] by making use of the potential functions and Hankel transforms. The problem of an elastic plate supported by an elastic two-parameter subgrade is studied in [Wen-da and Shu 1987] in order to model the circular foundation of a cooling hyperbolic tower. Results are compared with a numerical solution obtained through a FE package. The mechanical interaction between an infinite cracked Kirchhoff plate resting on a two-parameter elastic subgrade can be found in [Nobili et al. 2014, 2015]. A full-field solution is obtained therein by means of the Wiener–Hopf method and the influence of the subgrade parameters on the stress intensity factors at the crack tip are evaluated in detail.

Recently, Shukla et al. [2011] have obtained the solution of a circular plate supported by a tensionless Pasternak-type subgrade by using the strain energy approach and assuming a power series expansion for the transverse deflection of the plate. Variational boundary conditions for a beam resting on a two-parameter tensionless elastic foundation have been developed in [Nobili 2012]. Shell- and plate-like elements in contact with elastic media have been adopted as a reliable model to study micro- or nano-structures in the framework of modern microelectronics based on the use of special composite materials. As an example, Ru [2001] studied the critical loading for a double-walled carbon nanotube embedded in an elastic matrix. There, the nanotube is modeled as a thin elastic cylindrical shell supported by a Winkler subgrade, which accounts for the van der Waals forces. Likewise, in order to investigate the vibrations of carbon nanotubes, Liew et al. [2006] consider a plate embedded into a Pasternak elastic medium and solve the problem by means of Fourier analysis. It is found that the resonant frequencies of the system can be significantly affected by van der Waals interaction. Later, Pradhan and Kumar [2010] extended the vibration analysis to orthotropic single layered graphene sheets, taking into account scale effects by adopting Eringen nonlocal constitutive relations for the plate. These authors extend a previous work by Duan and Wang [2007] concerning the axisymmetric bending of circular plates under static loading and find that scale effects can produce a decrease of stiffness and, in turn, larger deflection of the plate.

Numerical simulations have been extensively adopted to study plate and slabs supported by or embedded in an elastic medium. As an example, Çelik and Saygun [1999] develop an iterative FE numerical method to simulate a plate on a two-parameter foundation. In that study, the soil surrounding the plate has been modeled by a finite region having amplitude comparable with the thickness of the compressible soil layer underneath the plate. Caliendo and Parisi [2010] studied the stress field in jointed concrete airport pavements under aircraft loads and thermal gradients. Through a commercial FE package, the authors carried out 3D numerical simulations wherein the pavement is modeled as a square-shaped plate bonded to an isotropic elastic half-space, thus incorporating the effect of the subgrade Young modulus on the maximum tensile stress at the interior as well as at the edge of the plate. A recent application of a FE-boundary integral equation coupling method is adopted in [Tullini et al. 2012] to investigate the interaction problem between a bar and an elastic half-plane. In this work, the Green function of the half-plane is implemented in the variational formulation.

Analytical and numerical models based on plates supported by an elastic subgrade can be readily used to simulate insulated building foundation. In fact, in order to adequately insulate the base of a building with the aim to reduce heat loss and, in turn, cut down on energy cost, an insulating layer (typically, high-compressive-strength polystyrene sheets and foams) can be placed right under the foundation concrete slab. Through this layer, moisture absorption, humidity infiltration and frost penetration phenomena are

hampered, the latter being a relevant issue in frost-susceptible soils [Bowles 1997]. The contribution of the insulating layer to the pressure distribution under the foundation is usually neglected, but it can be properly considered by adopting a two-parameter soil model.

Despite its potential and simplicity, linear elastic analysis cannot be used to predict the mechanical behavior of systems under the collapse load, when nonlinearity plays an essential role. In particular, models based on plasticity theory have been widely used to assess the load carrying capacity of mat building foundations. One of the first studies concerning the load-carrying capacity of rigid-plastic plates supported by a Winkler subgrade under a uniform static loading distribution was performed by Meyerhof [1960; 1962]. He assumed a fan-like collapse mechanism for the plate and thus he found an upper-bound for the collapse load, since the corresponding radial bending moment overcomes the yield moment of the plate. After those studies, a lot of works about this topic have appeared in the literature. By using potential functions to represent stress and displacements fields of the foundation, Gazetas [1981b] studied a transversely isotropic elastic half-space indented by a rigid-plastic plate under a uniform load distribution. He considered a conical shape of the plate after yielding, which can lift off the foundation. Sokół-Supel [1985; 1988] studied elastic-plastic Kirchhoff plates resting on an elastic subgrade. Solutions of elastic-plastic plates under different loading conditions and variously clamped at the ends may be found in the book by Save et al. [1997]. Lewandowski and Świtka [1991] solved the problem of a plate in tensionless contact with an underlying elastic-plastic Winkler subgrade obeying a bilinear constitutive law via a variational formulation. The authors solved the problem by using a FE method implemented through an iterative procedure. Kocatürk [1997] considered an elastic perfectly plastic plate in tensionless contact with an elastic-plastic Winkler foundation.

Recently, the problem of an infinite elastic-plastic plate resting on an elastic Winkler-type subgrade and uniformly loaded on a circular area has been solved by Radi and Di Maida [2014] by assuming the Johansen yield criterion for the plate [Johansen 1962] and associative flow rule. In that work, the exact ultimate bearing capacity of the system has been assessed varying the radius of the loaded region. It is also shown that the behavior of the plate is governed by a single parameter, namely the amplitude of the loaded region over the characteristic length of the plate-foundation system, and an approximate formula for the collapse load is also proposed.

Then, the study has been extended by Lanzoni et al. [2014] by considering a nonlocal behavior of the soil. In that study, a two-parameter foundation with a specific value of the Pasternak modulus has been assumed, resulting in closed-form solutions of the governing equations for the elastic-plastic regions that may occur within the plate. The analysis shows that the collapse mechanism of the plate differs from that found by Radi and Di Maida [2014], due to the nonlocal response of the Pasternak foundation.

The present work is the natural extension of the work by Lanzoni et al. [2014]. Here a general value of the Pasternak modulus is taken into account and the effects of the subgrade on the load-bearing capacity of the plate are investigated. A method based on a contour integral is adopted to solve in closed form the fourth-order linear ODE with nonconstant coefficients governing the mechanical behavior within the elastic-plastic region of the plate.

It is remarked that the plate is perfectly bonded to the elastic subgrade, thus the reactive soil pressure can be compressive as well as tensile. The study concerns the mechanical behavior of the system at the onset of plastic collapse. Nonetheless, it is worth noting that the system can sustain further increases in the external load after the plastic mechanism is achieved, owing to the presence of the elastic subgrade.

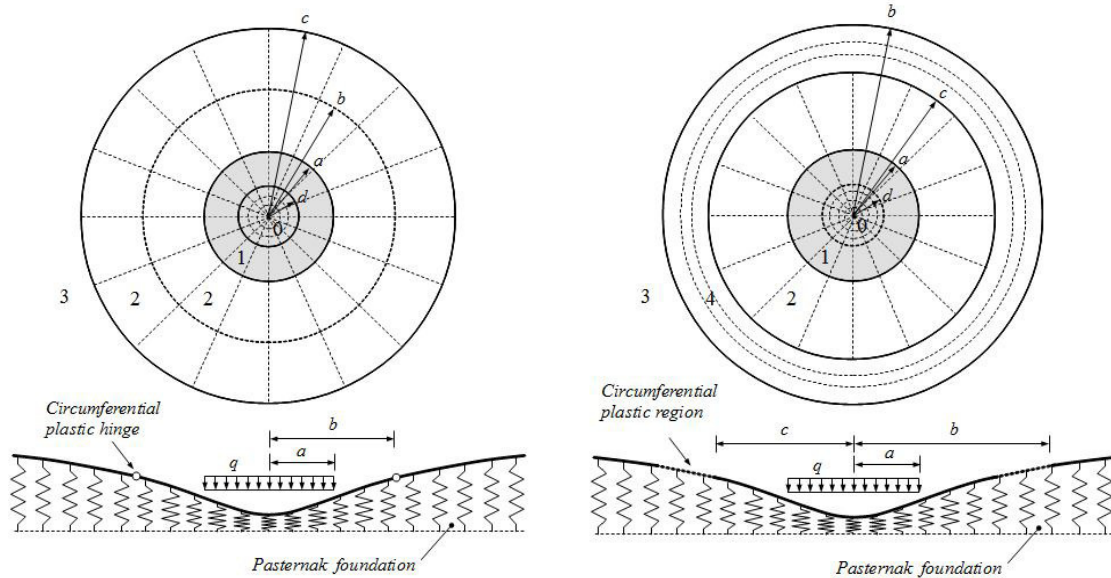


**Figure 1.** Sketch of the plastic mechanism for  $b < c$  (left) and for  $c < b$  (right). The loaded region  $0 \leq r \leq a$  has been highlighted. (0) plastic corner region  $r \leq d$ ; (1) elastic-plastic region under load  $d \leq r \leq a$ ; (2) unloaded elastic-plastic region; (3) elastic outer region; (4) annular elastic-plastic region.

The paper is organized as follows. Section 2 deals with the governing ODEs for the elastic-plastic regions that may arise within the plate. Solutions of these ODEs are found for a general value of the Pasternak subgrade modulus. The boundary conditions for each considered collapse mechanism are set in Section 3. The main results are reported in Section 4 in terms of ultimate load-bearing capacity, bending moments, shear forces, reactive soil pressure together with the size of each subregion. An experimental setup is briefly presented in Section 5. Finally, conclusions are drawn in Section 6.

## 2. Governing equations

In this section, the governing equations adopted in [Lanzoni et al. 2014] are briefly reviewed. The plate is subject to an external uniform pressure distribution  $q$  acting on its upper surface within a circular area of radius  $a$  and positive in the downward direction (see Figure 1). Elastic-perfectly plastic and isotropic behavior is adopted for the plate, which is assumed to obey Johansen's yield condition with associative flow rule. Due to the axisymmetrical conditions affecting the system, all variables depend on the radial coordinate  $r$  only.

The plate rests on an elastic two-parameter Pasternak foundation. Therefore, the reactive soil pressure  $p$  (positive if upwards) reads

$$p = k_1 w - k_2 \Delta w, \quad (1)$$

where  $k_1$  and  $k_2$  are the (positive) subgrade moduli,  $w$  represents the transversal deflection (positive if downward), and  $\Delta$  is the Laplacian operator in two dimensions.

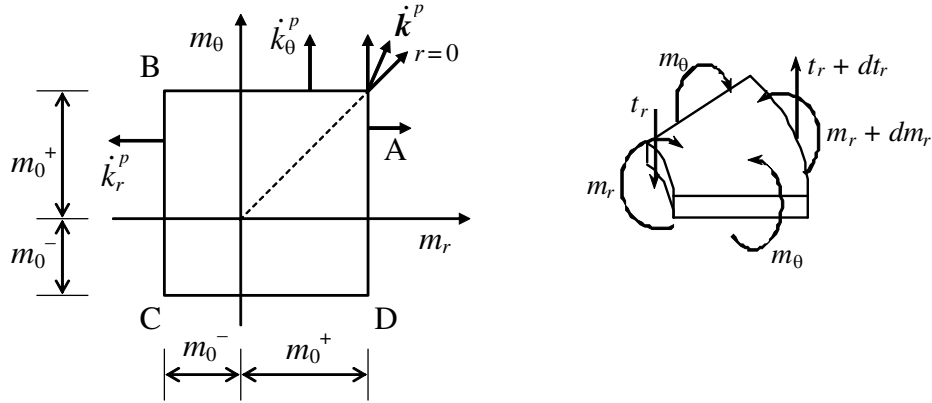


**Figure 2.** Left: Johansen's yield locus for elastic-plastic plates and corresponding flow rule. Right: positive bending moments and shear force per unit length.

Both in the elastic and in the elastic-plastic regions of the plate, the equilibrium conditions under axisymmetric loading conditions require

$$(rm_r)' - m_\theta + rt_r = 0, \quad (2)$$

$$(rt_r)' + r[k_1 w - k_2(w'' + w'/r) - q] = 0, \quad (3)$$

where  $m_r$  and  $m_\theta$  are the bending moments per unit length,  $t_r$  is the transverse shear force per unit length, whose positive directions are shown in Figure 2, right, and prime denotes differentiation with respect to the radial coordinate  $r$ .

Johansen's square yield condition is assumed to hold for the plate (Figure 2, left), namely

$$-m_0^- \leq m_r \leq m_0^+, \quad -m_0^- \leq m_\theta \leq m_0^+, \quad (4)$$

where  $m_0^+$  and  $m_0^-$  are the positive and negative yield moments per unit length.

Under proportional loadings, the elastic-plastic constitutive equations can be assumed in the integrated form

$$m_r = D(k_r^e + \nu k_\theta^e), \quad m_\theta = D(k_\theta^e + \nu k_r^e), \quad (5)$$

where  $k_r$  and  $k_\theta$  are the components of the curvature tensor,  $D = Eh^3/12(1 - \nu^2)$  is the flexural rigidity of the plate,  $h$  is the plate thickness,  $E$  is the Young's modulus and  $\nu$  is the Poisson's coefficient of the material. The curvature tensor can be separated into elastic and plastic contributions according to

$$k_r = k_r^e + k_r^p = -w''(r), \quad k_\theta = k_\theta^e + k_\theta^p = -w'(r)/r, \quad (6)$$

where the elastic components of the curvature tensor follow from (5) as

$$k_r^e = \frac{m_r - \nu m_\theta}{D(1 - \nu^2)}, \quad k_\theta^e = \frac{m_\theta - \nu m_r}{D(1 - \nu^2)}. \quad (7)$$

Following the classical Kirchhoff theory for thin plates, the rotation of the cross-sections of the plate orthogonal to the radial direction can be evaluated through the derivative of the displacement with respect

to the radial coordinate, i.e.,

$$\phi_\theta = -w'. \quad (8)$$

In the following, a dimensionless parameter  $\xi$  is introduced to make clear the role of the Pasternak stiffness parameter  $k_2$ , leading to a useful normalization of the ODEs governing the problem:

$$k_2 = \xi k_1 L^2, \quad (9)$$

where

$$L = \sqrt[4]{D(1 - \nu^2)/k_1} \quad (10)$$

is a characteristic length of the plate/subgrade system. It follows that, for  $\xi \rightarrow 0$ , the Winkler foundation is retrieved.

As found in [Lanzoni et al. 2014], the plate at the onset of collapse may exhibit two different plastic mechanisms, characterized by different elastic-plastic regions. For the sake of clarity, the governing equation for the transversal deflection of the plate and the corresponding solutions for each plastic region are presented in the following, the numbering of the letters being presented in Figure 1.

**2.1. Elastic-plastic region 0 lying at the corner A of the yield surface ( $0 \leq r \leq d$ ).** Due to the axisymmetry of the problem, the conditions

$$m_r(0) = m_\theta(0), \quad k_r^p(0) = k_\theta^p(0) \quad (11)$$

are met for  $r = 0$ . Moreover, the condition

$$m_r(r) = m_\theta(r) = m_0^+ \quad \text{for } 0 \leq r \leq d \quad (12)$$

must hold within the central region of the plate lying on the corner A of the yield surface. It is worth noting that the yield locus is not smooth and the plastic flow can assume different directions at the corner of the yield surfaces. However, the condition  $m_r(0) = m_\theta(0)$  holds at the center of the plate due to axisymmetry and, thus, also the plastic contributions of the curvature tensor are expected to be equal, i.e.,  $k_r^p(0) = k_\theta^p(0)$ , according to (11). On the other hand, the condition  $m_\theta(r) = m_0^+$  holds within the elastic plastic regions 1 and 2, namely for  $d < r < b$ , together with the normality law for the plastic flow  $k_\theta^p(r) > 0$  and  $k_r^p(r) = 0$ , so that the flow of the plastic curvature is aligned with the outward normal to the boundary AB of the yield domain, according to the Johansen associative yield criterion, as shown in Figure 2, left. Thus, within the fully plasticized region (region 0), the plastic flow must lie arbitrarily in the cone delimited by the bisector (OA direction) and the outward normal to the boundary AB of the strength domain.

This assumption leads to the fulfillment of the maximum dissipation postulate also at the corner A of the yield domain [Salençon 2013, Chapter 11.3.2]. In particular, the plastic curvature  $k_\theta^p(r)$  is assumed to vary continuously with  $r$  from the center of the plate ( $r = 0$ ) where  $k_\theta^p(0) = k_r^p(0)$  to the outer border of the region 0 ( $r = d^-$ ) where  $k_\theta^p(d^-) = k_\theta^p(d^+)$ , so that the circumferential component of the plastic curvature tensor is continuous between the regions 0 and 1. As discussed in [Lanzoni et al. 2014], continuity of this component also implies continuity of the rotation  $\phi_\theta$  between the regions 0 and 1 at  $r = d$ , according to relation (6)<sub>2</sub>, since the elastic component of the curvature is continuous due to the continuity of the bending moments.



The yield condition (12) and the balance equation (2) imply the vanishing of the transverse shear force within the inner elastic-plastic region 0, i.e.,

$$t_r(r) = 0 \quad \text{for } 0 \leq r \leq d, \tag{13}$$

and, thus, the load is entirely supported by the subgrade therein.

By using relations (9) and (13), the general expression for the transversal deflection of the plate within the elastic-plastic region 0 can be found from the balance condition (3) in the form

$$w_0(r) = (m_0^+ L^2 / D) [\chi + a_0 I_0(r / \sqrt{\xi} L)], \tag{14}$$

where  $I_0$  is the modified Bessel function of first kind of order zero,  $a_0$  is an arbitrary constant and

$$\chi = qD / (k_1 m_0^+ L^2) \tag{15}$$

is a dimensionless parameter proportional to the intensity  $q$  of the external load distribution.

**2.2. Elastic-plastic regions 1 and 2 lying on the side AB of the yield surface ( $d \leq r \leq c$ ).** On the side AB of the yield locus (Figure 2, left) the bending moment  $m_\theta$  attains its positive limit value  $m_0^+$ , namely

$$m_\theta(r) = m_0^+ \quad \text{for } d \leq r \leq c, \tag{16}$$

and thus positive radial yield lines occur within the corresponding elastic-plastic region of the plate, which can be split into the inner loaded region 1 and the outer unloaded region 2, as sketched in Figure 1. According to the associative flow rule, the plastic curvature components for the side AB of the yield locus are given by

$$k_r^p = 0, \quad k_\theta^p \geq 0. \tag{17}$$

Therefore, by using (16) and (17)<sub>1</sub>, equations (6)<sub>1</sub>, (7)<sub>1</sub> and (2) yield the following expressions for the bending moment  $m_r$  and the transverse shear force  $t_r$  per unit length in the elastic-plastic regions 1 and 2:

$$m_r = \nu m_0^+ - D(1 - \nu^2)w'', \tag{18}$$

$$t_r = \frac{1 - \nu}{r} [m_0^+ + D(1 + \nu)(w'' + rw''')]. \tag{19}$$

Introduction of (19) in the balance equation (3) then provides the governing ODE for these regions:

$$r w'''' + 2w''' - \frac{\xi}{L^2} w'' r - \frac{\xi}{L^2} w' + \frac{1}{L^4} w r - \frac{q}{k_1 L^4} r = 0. \tag{20}$$

The general solution of the fourth-order linear ODE (19) has been found in closed form by Lanzoni et al. [2014] only for the special case  $\xi = 2$ .

Different methods can be used to solve the ODE (20). For example, the solution can be obtained numerically, or by using the method of Frobenius, i.e., by seeking the unknown function  $w$  as a power series of  $r$  and solving the corresponding indicial equation. Here, we use a contour integration instead (see for example [Ince 1944]). Assume that  $w(r)$  has the form

$$w(r) = \int_C S(p) e^{pr/L} dp, \tag{21}$$

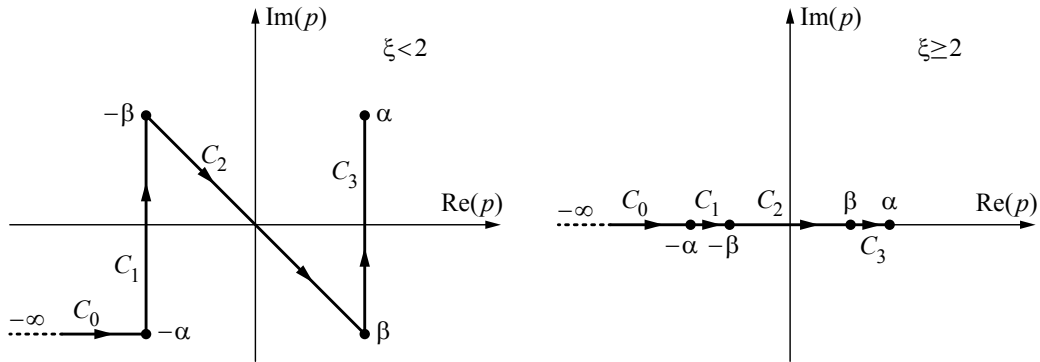


**Figure 3.** Path of integration in the complex domain for complex conjugate roots (left) and real roots (right).

where  $S(p)$  is an unknown function of the complex variable  $p$  and  $C$  a contour to be defined later. Therefore, introduction of the representation (21) in (20) and taking  $q = 0$  gives

$$\frac{r}{L} \int_C (p^4 - \xi p^2 + 1) S(p) e^{pr/L} dp + \int_C (2p^3 - \xi p) S(p) e^{pr/L} dp = 0. \tag{22}$$

Integration by parts of the first integral in (22) then yields

$$\int_C (2p^3 - \xi p) S(p) e^{pr/L} dp + \int_C (p^4 - \xi p^2 + 1) S'(p) e^{pr/L} dp - (p^4 - \xi p^2 + 1) S(p) e^{pr/L} \Big|_{p_i}^{p_f} = 0, \tag{23}$$

where prime denotes differentiation with respect to the function argument  $p$ . If the contour  $C$  is chosen in such a way that the last term vanishes, then the function  $S(p)$  must satisfy the ODE

$$(2p^3 - \xi p) S(p) + (p^4 - \xi p^2 + 1) S'(p) = 0, \tag{24}$$

namely,

$$\frac{S'(p)}{S(p)} = -\frac{(2p^3 - \xi p)}{(p^4 - \xi p^2 + 1)}. \tag{25}$$

Integration of (25) gives the general expression of the function  $S(p)$  as

$$S(p) = A(p^4 - \xi p^2 + 1)^{-1/2}, \tag{26}$$

where  $A$  is an arbitrary constant.

The contour  $C$  must be chosen in order to satisfy the condition

$$(p^4 - \xi p^2 + 1) e^{pr/L} \Big|_{p_i}^{p_f} = 0. \tag{27}$$

The latter condition is satisfied for  $p = \pm\alpha, \pm\beta$ , and for  $p \rightarrow -\infty$ , where

$$\alpha = \sqrt{\xi/2 + \sqrt{\xi^2/4 - 1}}, \quad \beta = \sqrt{\xi/2 - \sqrt{\xi^2/4 - 1}}, \tag{28}$$

and the contour  $C$  can be defined as sketched in Figure 3 for complex and real values of the variable  $p$ , respectively, in order to obtain four independent solutions of (20) in the form given by (21). Namely, the contours  $C_k$  ( $k = 1, 2, 3$ ) are chosen to coincide with the three straight paths joining the points

$-\alpha, -\beta, \beta, \alpha$  of the complex plane, respectively, and the fourth path is defined by  $C_0 = \{x - i\text{Im}(\alpha) \mid -\infty \leq x \leq -\text{Re}(\alpha)\}$ . Note that the roots (28) are real for  $\xi \geq 2$ , whereas they become complex conjugates for  $\xi \leq 2$  (see Figure 3). Therefore, the function  $w(r)$  can be assumed in the form

$$w_1(r) = \frac{m_0^+ L^3}{D} \left[ \frac{\chi}{L} + \sum_{k=0}^3 b_k \int_{C_k} \frac{e^{pr/L}}{\sqrt{p+\alpha}\sqrt{p+\beta}\sqrt{p-\alpha}\sqrt{p-\beta}} dp \right] \quad \text{for } d \leq r \leq a. \quad (29)$$

Equation (29) defines the displacement field within the annular loaded region, whereas the displacement field within the elastic-plastic annular region not directly loaded (namely for  $q = 0$ ) is given by

$$w_2(r) = \frac{m_0^+ L^3}{D} \sum_{k=0}^3 c_k \int_{C_k} \frac{e^{pr/L}}{\sqrt{p+\alpha}\sqrt{p+\beta}\sqrt{p-\alpha}\sqrt{p-\beta}} dp \quad \text{for } a \leq r \leq c. \quad (30)$$

**2.3. Elastic-plastic region 4 lying on the side BC of the yield surface ( $c \leq r \leq b$ ).** On the side BC of the yield locus (Figure 2, left) the bending moment  $m_r$  attains its negative limit value, namely

$$m_r(r) = -m_0^- \quad \text{for } c \leq r \leq b, \quad (31)$$

according to the associative flow rule, and thus negative circumferential yield lines occur within the corresponding elastic-plastic region 4 in Figure 1, right, where  $c \leq r \leq b$ . The plastic curvature components are given by the associative flow rule for the side BC of the yield locus, namely,

$$k_r^p \leq 0, \quad k_\theta^p = 0. \quad (32)$$

Therefore, from (6)<sub>2</sub>, (7)<sub>2</sub> and (32)<sub>2</sub> the bending moment per unit length  $m_\theta$  in the present elastic-plastic region reads

$$m_\theta = -\nu m_0^- - D(1 - \nu^2)w'/r. \quad (33)$$

Then, from (2) and (33) the transverse shear force per unit length follows as

$$t_r = \frac{1 - \nu}{r} [m_0^- - D(1 + \nu)w'/r]. \quad (34)$$

Substitution of (34) in the balance equation (3), also using (9), then yields the governing equation in terms of displacement for the elastic-plastic region 4 as

$$\left(1 + \xi \frac{r^2}{L^2}\right) w'' - \left(1 - \xi \frac{r^2}{L^2}\right) \frac{w'}{r} - \frac{r^2}{L^4} w = 0. \quad (35)$$

The general solution of the fourth-order linear ODE (35) in closed form is

$$w_4(r) = \frac{m_0^+ L^2}{D} \sqrt{2/\xi} \left[ a_1 I_0\left((1/\xi)\sqrt{1 + \xi r^2/L^2}\right) + a_2 K_0\left((1/\xi)\sqrt{1 + \xi r^2/L^2}\right) \right], \quad (36)$$

where  $K_0$  is the modified Bessel function of the second kind of order zero [Abramowitz and Stegun 1972], and  $a_1$  and  $a_2$  are arbitrary constants.

**2.4. Elastic region 3.** The governing differential equation in terms of the transversal displacement  $w(r)$  for the elastic region 3 of the plate under symmetrical bending reads

$$w'''' + \frac{2}{r}w'''' - \frac{1}{r^2}w'' + \frac{1}{r^3}w' - a\left(w'' + \frac{1}{r}w'\right) + \frac{1-\nu^2}{L^4}w = 0, \quad (37)$$

where  $a = k_2/D = \xi(1-\nu^2)/L^2$ . It can be shown that, if  $\eta = aL^2/(2\sqrt{1-\nu^2}) \leq 1$ , the general solution of the ODE (37) as  $r$  becomes very large reads [Selvadurai 1979]

$$w_3(r) = \frac{m_0^+ L^2}{D} \{d_1 \operatorname{Re}[H_0^{(1)}(\beta r/L)] + d_2 \operatorname{Im}[H_0^{(1)}(\beta r/L)]\} \quad \text{for } r \geq c, \quad (38)$$

where  $H_0^{(1)}$  is the Hankel function of the first kind [Abramowitz and Stegun 1972],  $d_1$  and  $d_2$  are dimensionless real constants and

$$\beta = i\sqrt[4]{1-\nu^2}(\sqrt{\eta + \sqrt{\eta^2 - 1}}). \quad (39)$$

The general solution of the ODE (37) for  $\eta > 1$  reads

$$w_3(r) = \frac{m_0^+ L^2}{D} \{d_1 \operatorname{Re}[Y_0(i\beta_1 r/L)] + d_2 \operatorname{Re}[Y_0(i\beta_2 r/L)]\} \quad \text{for } r \geq c, \quad (40)$$

where

$$\beta_1 = \sqrt[4]{1-\nu^2}(\sqrt{\eta + \sqrt{\eta^2 - 1}}), \quad \beta_2 = \sqrt[4]{1-\nu^2}(\sqrt{\eta - \sqrt{\eta^2 - 1}}). \quad (41)$$

It is worth noting that, for  $\xi = 2/\sqrt{1-\nu^2}$ , the solution of the elastic region reported in [Lanzoni et al. 2014] is retrieved from (38).

The relationship between the curvature components and the bending moments per unit length is given by [Timoshenko and Woinowsky-Krieger 1959]

$$m_r = -D(w_3'' + (\nu/r)w_3'), \quad m_\theta = -D(w_3'/r + \nu w_3''), \quad (42)$$

whereas the expression of the shear force  $t_r$  per unit length reads

$$t_r = D(w_3''' + w_3''/r - w_3'/r^2). \quad (43)$$

### 3. Boundary conditions

The dimensionless constants  $a_0, d_1, d_2, b_0, b_1, b_2, b_3, c_0, c_1, c_2, c_3, a_1$  and  $a_2$  appearing in the expressions for the displacement in the different regions considered in Section 2 can be evaluated by imposing proper continuity conditions for the displacement  $w$ , rotation  $\phi_\theta$ , bending moment  $m_r$  and shear force  $t_r$  per unit length across the boundaries between the regions at  $r = a, c$  and  $d$ , together with the fulfillment of the yield condition at the inner boundary of the elastic region and the conditions about the occurrence of a plastic mechanism in the plate at the onset of collapse.

As discussed in [Lanzoni et al. 2014], two different plastic mechanisms may occur in the plate at the onset of collapse, depending on the amplitude  $a/L$  of the loaded region. Continuity of displacement  $w$ , rotation  $\phi_\theta$ , bending moment  $m_r$  and shear force  $t_r$  across the boundary at  $r = d$  and  $r = a$  must be

imposed for both plastic mechanisms as

$$w_0(d) = w_1(d), \quad w'_0(d) = w'_1(d), \quad D(1 + \nu)w''_1(d) = -m_0^+, \quad w'''_1(d) = 0, \quad (44)$$

$$w_1(a) = w_2(a), \quad w'_1(a) = w'_2(a), \quad w''_1(a) = w''_2(a), \quad w'''_1(a) = w'''_2(a), \quad (45)$$

where expressions (8), (18) and (19) have been used. One kind of plastic mechanism takes place with  $b < c$  (see Figure 1, left). In this case, continuity across the boundaries at  $r = c$  requires the further four conditions

$$\begin{aligned} w_2(c) &= w_3(c), \quad w'_2(c) = w'_3(c), \\ \frac{\nu m_0^+}{D} - (1 - \nu^2)w''_2(c) &= -w'''_3(c) - \frac{\nu}{c}w'_3(c), \\ (1 - \nu)\frac{m_0^+}{D} + (1 - \nu^2)[w''_2(c) + cw'''_2(c)] &= cw'''_3(c) + w'''_3(c) - \frac{1}{c}w'_3(c), \end{aligned} \quad (46)$$

where (8), (18), (19), (42)<sub>1</sub> and (43) have been used. Making use of (42)<sub>2</sub>, accomplishment of the yield condition as  $r$  approaches  $c$  from the outer elastic region requires

$$\nu w''_3(c) + \frac{1}{c}w'_3(c) = -\frac{m_0^+}{D}. \quad (47)$$

Moreover, the negative circumferential yield line must take place within the elastic-plastic region, i.e., at  $r = b$ , where  $d \leq b \leq c$ . In this case, the onset of collapse occurs when the bending moment  $m_r$  within the elastic-plastic region attains a minimum value equal to the ultimate negative bending moment right at  $r = b$ , i.e.,

$$D(1 - \nu^2)w''_2(b) = (\nu + \mu)m_0^+, \quad w'''_2(b) = 0, \quad (48)$$

for  $b \leq c$ , where

$$\mu = m_0^- / m_0^+ \quad (49)$$

is the ratio between negative and positive yield moments.

Conditions (44)–(48) yield a system of 15 equations, which are linear in the 12 constants  $a_0, b_0, b_1, b_2, b_3, c_0, c_1, c_2, c_3, d_1, d_2$  and  $\chi$ . Once 12 such quantities are found in terms of the radii  $b, c$  and  $d$ , the last three equations can be solved numerically in order to obtain the remaining unknowns  $b, c$  and  $d$ . Finally, the collapse load  $P$  of the plate follows from (15) as

$$P = \pi a^2 \chi k_1 m_0^+ L^2 / D. \quad (50)$$

The other possible scenario of plastic collapse occurs for  $b > c$ , namely when the negative circumferential yield line first appears within the elastic region (see Figure 1, right). In this case, the collapse load can be found by imposing the continuity conditions between the inner elastic-plastic region 2 and the annular elastic-plastic region 4 at  $r = c$ , where

$$\begin{aligned} w_2(c) &= w_4(c), \quad w'_2(c) = w'_4(c), \\ D(1 - \nu^2)w''_2(c) &= m_0^- + \nu m_0^+, \\ D(1 - \nu^2)\left[cw'''_2(c) + \frac{1}{c}w'_4(c)\right] + (m_0^+ + \nu m_0^-) &= 0, \end{aligned} \quad (51)$$

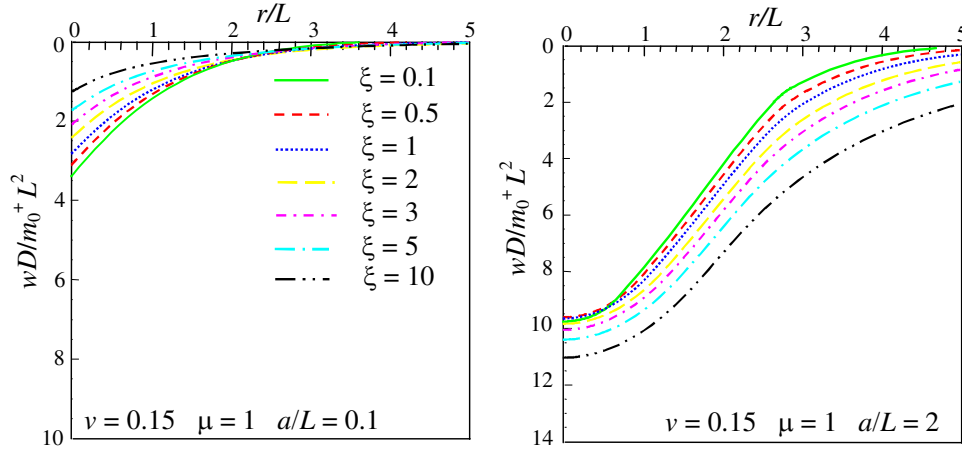


**Figure 4.** Radial variation of the dimensionless plate deflection for  $\mu = 1$ , varying the parameter  $\xi$  of the soil, for  $a/L = 0.1$  (left) and  $a/L = 2$  (right).

as well as between the annular elastic-plastic region 4 and the outer elastic region 3 at  $r = b$ , where

$$\begin{aligned} w_3(b) &= w_4(b), & w_3'(b) &= w_4'(b), \\ D \left[ w_3''(b) + \frac{\nu}{b} w_3'(b) \right] &= m_0^-, \\ D \left[ w_3'''(b) + \frac{1}{b} w_3''(b) - \frac{1}{b^2} w_3'(b) \right] &= \frac{1-\nu}{b} \left[ m_0^- - \frac{1}{b} D(1+\nu) w_4'(b) \right]. \end{aligned} \quad (52)$$

By using (52)<sub>2</sub>, (42)<sub>2</sub> and (33), Equation (52)<sub>3</sub> implies continuity of the bending moment  $m_\theta$  (and vice versa) across the boundary at  $r = b$ . Condition (52)<sub>4</sub> also implies the stationarity of the bending moment  $m_r$  within the elastic region at  $r = b$ .

Continuity of the bending moment  $m_\theta$  across the boundary at  $r = c$  must be imposed by using (33), thus giving

$$m_0^+ + \nu m_0^- + D(1-\nu^2) \frac{w_4'(c)}{c} = 0. \quad (53)$$

The substitution of the functions  $w_k(r)$  ( $k = 0, 1, 2, 3, 4$ ) introduced in Section 2 and their derivatives in conditions (44), (45), (51), (52) and (53) yield a system of 17 equations, which are linear in the 14 constants  $a_0, a_1, a_2, b_0, b_1, b_2, b_3, c_0, c_1, c_2, c_3, d_1, d_2$  and  $\chi$ . Once such constants are found in terms of the radii  $b, c$  and  $d$ , the numerical solution of the last three equations provides the values of  $b, c$  and  $d$ . Finally, the collapse load  $P$  of the plate can be calculated by using (50).

#### 4. Results

In the following, the radial variation of transverse displacement, slope, bending moments, shear force and reactive soil pressure at the onset of plastic collapse are reported and discussed. For the sake of definiteness, we assumed  $\nu = 0.15$ . The radial variation of the transverse deflection of the plate  $wD/m_0^+ L^2$  for different values of the subgrade parameter  $\xi$  has been reported in Figure 4 for  $a/L = 0.1$  and 2. Note that, if the Winkler modulus  $k_1$  and the flexural rigidity of the plate  $D$  are kept constant, the variation of

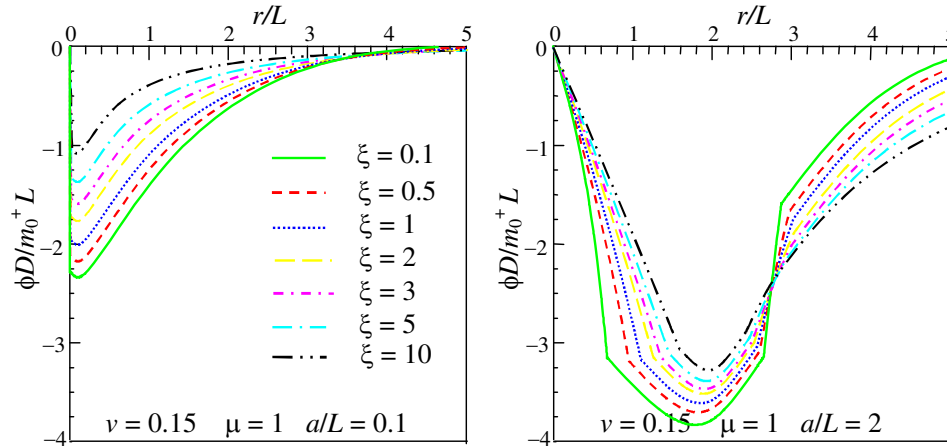


**Figure 5.** Radial variation of the dimensionless rotation of the plate cross-section for  $\mu = 1$ , varying the parameter  $\xi$  of the soil, for  $a/L = 0.1$  (left) and  $a/L = 2$  (right).

the parameter coincides with the variation of the Pasternak modulus  $k_2$ , where  $\xi = k_2/(k_1 L^2)$ , according to (9) and (10). As shown in Figure 4, left, for small sizes of the loaded region, the plate deflection under the loaded region monotonically decreases as  $\xi$  increases, whereas an opposite trend is observed for large sizes of the loaded region, as depicted in Figure 4, right. This effect is due to the fact that the reaction of the Pasternak foundation also depends on the first and second derivatives of the transverse deflection. In particular, the variation of the slope and, in turn, the second derivative of the displacement, assumes negative values in the inner region of the plate, and decreases going outward from the loaded region, as shown in Figure 5. Thus, in the inner region of the plate, the reactive soil pressure is compressive and very high for small sizes of the loaded region (see also Figure 9). Moreover, for large sizes of the loaded region, the slope displays a rapid variation out of the loaded area (from Figure 5, right, plotted for  $a/L = 2$ , it occurs approximately for  $r/L = 3$ ). It follows that, in the neighborhood of this region, the second derivative becomes positive and, thus, the soil reaction tends to become tensile due to the second term in (1). Consequently, as the parameters  $k_2$  and  $\xi$  increase while keeping constant the Winkler modulus  $k_1$ , the soil reaction becomes tensile out of the loaded region for large values of  $a/L$ , thus producing an increase in the transverse deflection of the plate, as shown in Figure 4, right. This effect does not occur for small values of  $a/L$ . In this case, an increase in the parameter  $\xi$  corresponds to a decrease of the displacement of the system, as revealed by Figure 4, left.

The radial variation of the slope  $\phi_\theta$  is shown in Figure 5 for  $a/L = 0.1, 2$ . The magnitude of the slope decreases under the loaded region as the Pasternak modulus  $k_2$  and the parameter  $\xi$  become larger, whereas an opposite trend is observed out of the loaded region for large sizes of the loaded region (Figure 5, right). Note also that the function  $\phi_\theta(r)$  is continuous, as required by the boundary conditions, but not monotonic, since its magnitude exhibits a maximum near the border of the loaded region.

The radial variations of bending moments  $m_r(r)$  and  $m_\theta(r)$  along the radial direction are plotted in dimensionless form in Figures 6 and 7 for different values of the parameter  $\xi$ . As shown in Figure 7, the circumferential bending moment  $m_\theta(r)$  attains the positive yield limit  $m_0^+$  within a circular region whose radius  $c$  increases with the size  $a$  of the loaded region and decreases as the parameter  $\xi$  becomes larger. Radial yield lines occur within this region.

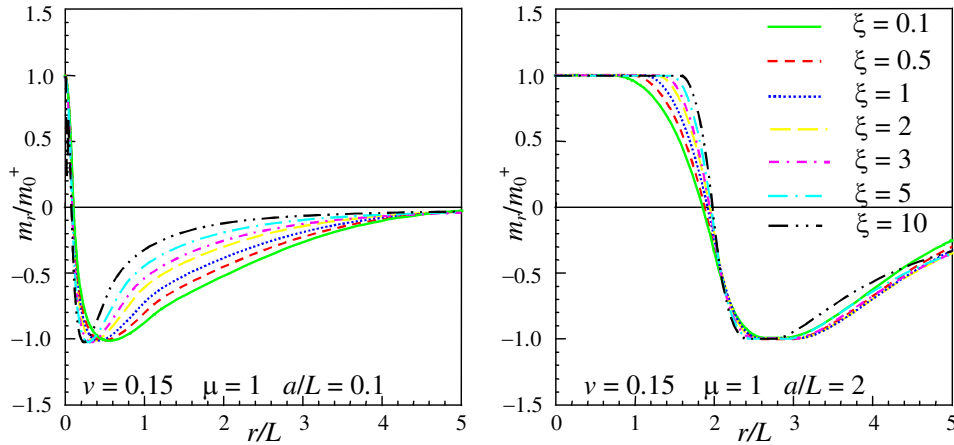


**Figure 6.** Radial variation of the dimensionless radial bending moment for  $\mu = 1$ , varying the parameter  $\xi$  of the soil, for  $a/L = 0.1$  (left) and  $a/L = 2$  (right).

For small sizes of the loaded area, the radial bending moment  $m_r(r)$  displays a positive peak just at the center of the loaded area where the positive yield moment  $m_0^+$  is attained (Figure 6, left) and then decreases outwards till the negative yield moment  $m_0^-$  is reached at  $r = b$ , where a negative circumferential yield line develops within region 2 and triggers the collapse mechanism within the plate. It is worth noting that the radius  $b$  of the negative circumferential yield line becomes smaller as the parameter  $\xi$  increases (Figure 6, left). For large sizes of the loaded area  $a$ , a circular region where both radial and circumferential bending moments attain the positive yield limit appears and extends outwards (Figure 6, right) as the size of the loaded region is increased. Both radial and circumferential yield lines take place within this region 0 of radius  $d$ . The amplitude of this fully yielded region at the onset of collapse increases with  $\xi$ , as shown in Figure 6, right. Out of this region, the radial bending moment  $m_r(r)$  decreases and becomes negative. The negative yield moment  $m_0^-$  is then reached within an annular

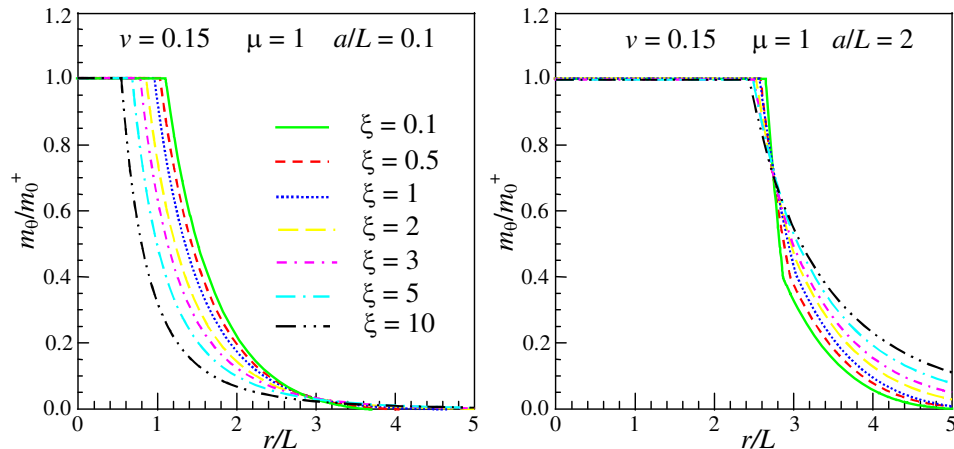


**Figure 7.** Radial variation of the dimensionless circumferential bending moment for  $\mu = 1$ , varying the parameter  $\xi$  of the soil, for  $a/L = 0.1$  (left) and  $a/L = 2$  (right).



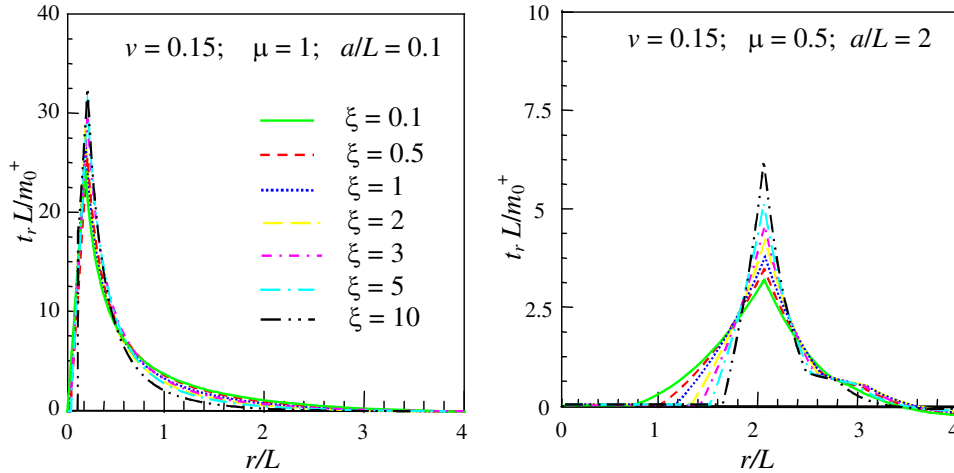


**Figure 8.** Radial variation of the dimensionless shear force for  $\mu = 1$ , varying the parameter  $\xi$  of the soil, for  $a/L = 0.1$  (left) and  $a/L = 2$  (right).

region, whose width increases with the load until it joins together with the inner radially yielded region, thus creating a plastic mechanism within the plate.

The bending moments within the outer elastic region decrease until they vanish at a large distance from the loaded area. For small sizes of the loaded area, the rate of decrease is faster for large values of the Pasternak modulus, i.e., of the parameter  $\xi$ , whereas for large sizes of the loaded area an opposite trend is observed.

The radial variations of shear force are plotted in Figure 8 in dimensionless form. These variations show a peak near the border of the loaded area, whose magnitude increases with the Pasternak modulus  $k_2$ . This behavior is expected since a stiffer foundation requires a larger applied load in order to achieve a plastic mechanism, thus producing an increase in the maximum shear force.

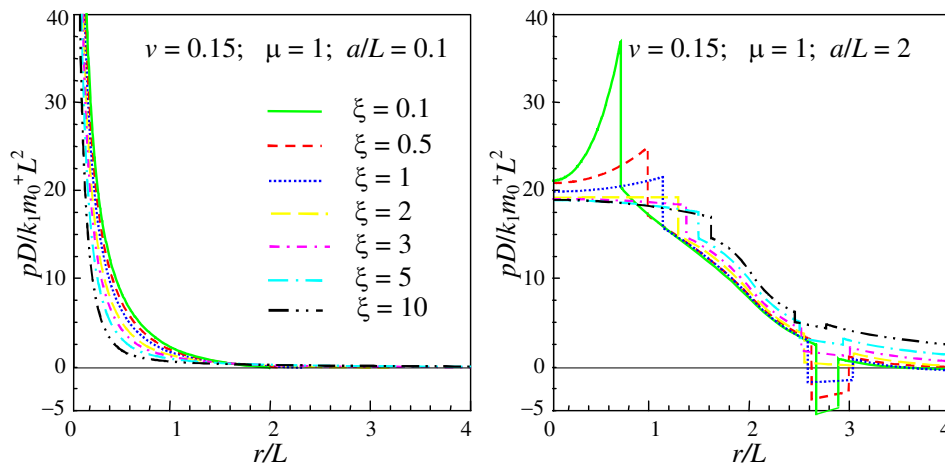


**Figure 9.** Radial variation of the dimensionless reacting soil pressure for  $\mu = 1$ , varying the parameter  $\xi$  of the soil, for  $a/L = 0.1$  (left) and  $a/L = 2$  (right).

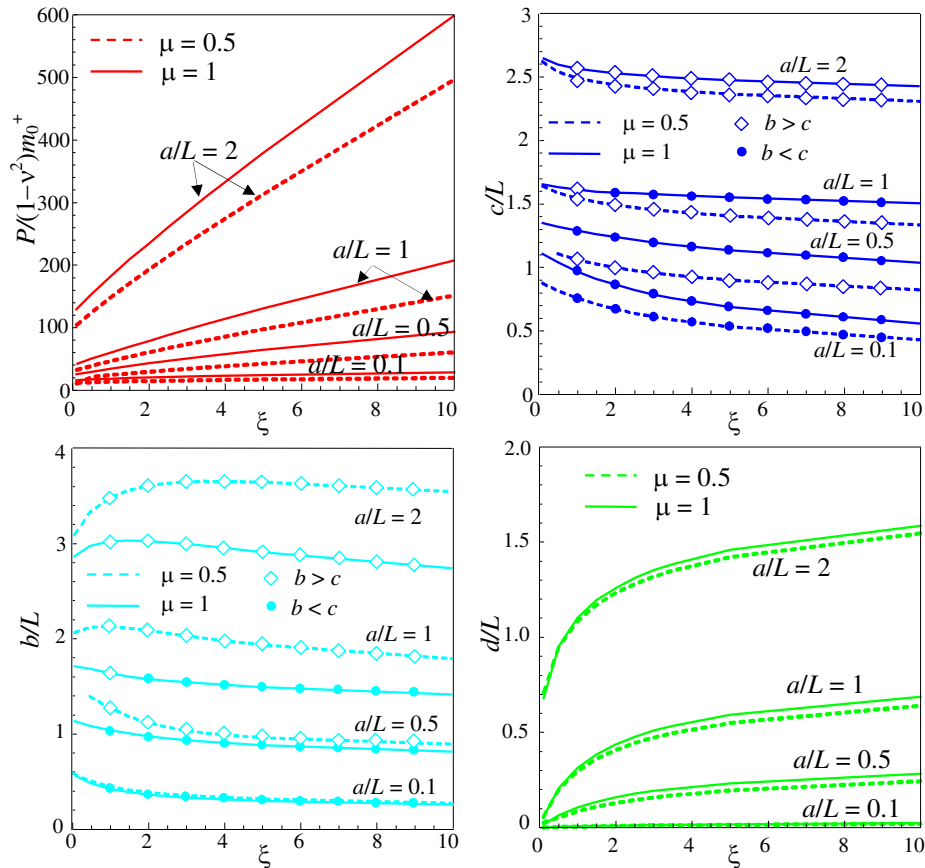


**Figure 10.** Top left: dimensionless ultimate load and dimensionless loci. Top right:  $x/L$ . Bottom left:  $y/L$ . Bottom right:  $d/L$  versus the parameter  $\xi$  of the soil for different values of the amplitude  $a$  of the loaded region, for  $\mu = 0.5, 1$ .

An interesting trend is observed for the curves of the reacting pressure, depicted in Figure 9. As the Pasternak modulus increases, the reactive soil pressure increases under the loaded region and decreases outside that region. In particular, Figure 9, right, highlights an increase of the peak of the soil pressure near the edge of region 0 for low values of the parameter  $\xi$ . This is due to the fact that the reacting pressure of the Pasternak soil depends on the Laplacian of the transverse deflection, namely on the slope and curvature. The latter exhibits a rapid variation at the border of region 0, as proved by the corner in the curves of Figure 5, right, and by the drop of the bending moment  $m_r$  from  $m_0^+$  to  $m_0^-$  shown in Figure 6, right.

Figure 10, top left, displays the dimensionless ultimate load versus  $\xi$  for some values of the amplitude  $a/L$  of the loaded region, both for  $\mu = 1$  and 0.5. As expected, the ultimate carrying capacity of the system increases with the soil stiffness for every value of the ratio  $a/L$ , as confirmed by the monotonic trend of the curves plotted in Figure 10, top left. If the parameters  $m_0^+$ ,  $a/L$  and  $\xi$  are kept constant, the collapse load obviously decreases as  $\mu$  decreases and thus  $m_0^-$  is reduced. Indeed, a decrease in  $\mu$  implies a reduction of the negative yield moment  $m_0^-$ , thus allowing the activation of the collapse

mechanism at a lower level of the external load. The variations of the ratios  $c/L$ ,  $b/L$  and  $d/L$  versus  $\xi$  are plotted in Figure 10 (top right, bottom left, bottom right, respectively). In particular, the dimensionless radius  $c/L$  monotonically decreases as the stiffness parameter  $\xi$  increases, whereas the variation of the radius  $b/L$  with  $\xi$  is not monotonic, as shown in Figure 10, top right and bottom left. These figures show also that the border of the elastic-plastic region (i.e., the radius  $c$  or  $b$  of the plastic mechanism for  $b < c$  or  $c < b$ , respectively) displays a nonmonotonic trend for large values of  $a/L$ , whereas for moderate values of  $a/L$  the amplitude of the elastic-plastic zone monotonically decreases as the parameter  $\xi$  increases. Note that, for  $a/L = 1$ , the collapse mechanism for  $b > c$  takes place for small values of the parameter  $\xi$  (approximately, until  $\xi \leq 1.5$ ). Increasing  $\xi$ , the collapse mechanism occurs for  $c > b$ . The parameter  $\mu$  significantly affects the size of the elastic-plastic region, mainly for large sizes of the loaded region, as shown by Figure 10, bottom left. Moreover, if the parameter  $\xi$  is kept constant, an increase in the parameter  $\mu$  produces a decrease (increase) of the size of the elastic-plastic region for large (small) values of the amplitude of the loaded region  $a/L$ . From Figure 10, bottom right, it can be recognized that the radius  $d$  increases monotonically with  $\xi$ . Note that the influence of the parameter  $\mu$  on  $c$  and  $d$  is lower than that found for radius  $b$ .

Finally, the variation of the ultimate load and ratios  $c/L$ ,  $b/L$ ,  $d/L$  versus  $\mu$  are plotted in Figure 11 for  $a/L = 0.5$  and for some values of the parameter  $\mu$ . Figure 11, top left, shows that the ultimate load increases monotonically both with  $\xi$  and  $\mu$ , as expected from an increase in the soil stiffness and negative yield moment. Figure 10, top right, shows that the radius  $c$  of the circumferential yield line becomes smaller as  $\mu$  becomes vanishing small, and its variation with the parameter  $\mu$  is monotonic. Conversely, the radius  $b$  of the circumferential yield line monotonically decreases as  $\mu$  increases (Figure 11, bottom left). Moreover, the analysis shows that there exists a specific value of  $\mu$  that minimizes the amplitude of the elastic-plastic region of the plate depending on the value of  $\xi$ . For  $a/L = 0.5$ , this occurs for values of  $\mu \leq 1$  regardless of the value of the soil stiffness  $\xi$ . However, the influence of the parameter  $\xi$  on the radii  $c$  and  $b$  is limited. As expected, the amplitude  $d$  of the fully yielded region 0 increases both with  $\mu$  and  $\xi$ , as confirmed by Figure 11, bottom right.

## 5. Experiments and possible applications

The model proposed here can be reliably used to predict the mechanical behavior of ductile elements (e.g., FRC slabs, metallic sheets, etc.) bonded to an elastic support under axisymmetric load distributions. For an example, it may be used to assess the failure mechanism of plastic or rubbery sheets covered by metallic thin films. This kind of composites finds important applications for many industrial purposes. For instance, plastic sheets coated by an aluminium film are widely used in the pharmaceutical, food and cosmetic industries to achieve hygienic packaging.

For example, Figure 12 shows a ductile polycarbonate sheet supported by a 6 mm thick sheet of rubber and coated by an Al thin film. The polycarbonate sheet is 5 mm thick, whereas the Al film thickness equals  $50 \mu\text{m}$ . A load distribution has been imparted to the sample by means of a hydraulic cylinder mounted into a suitable metallic frame. The Al film allows the identification of the occurrence of the yield lines. Indeed, in the neighborhood of the negative circumferential yield line, a detachment of the Al film occurs, thus producing small wrinkles, as shown in Figure 12, top right. In the proximity of positive radial yield lines, radial cracks within the Al film can also be detected (see Figure 13). These findings thus confirm the plastic mechanisms investigated in the present work.

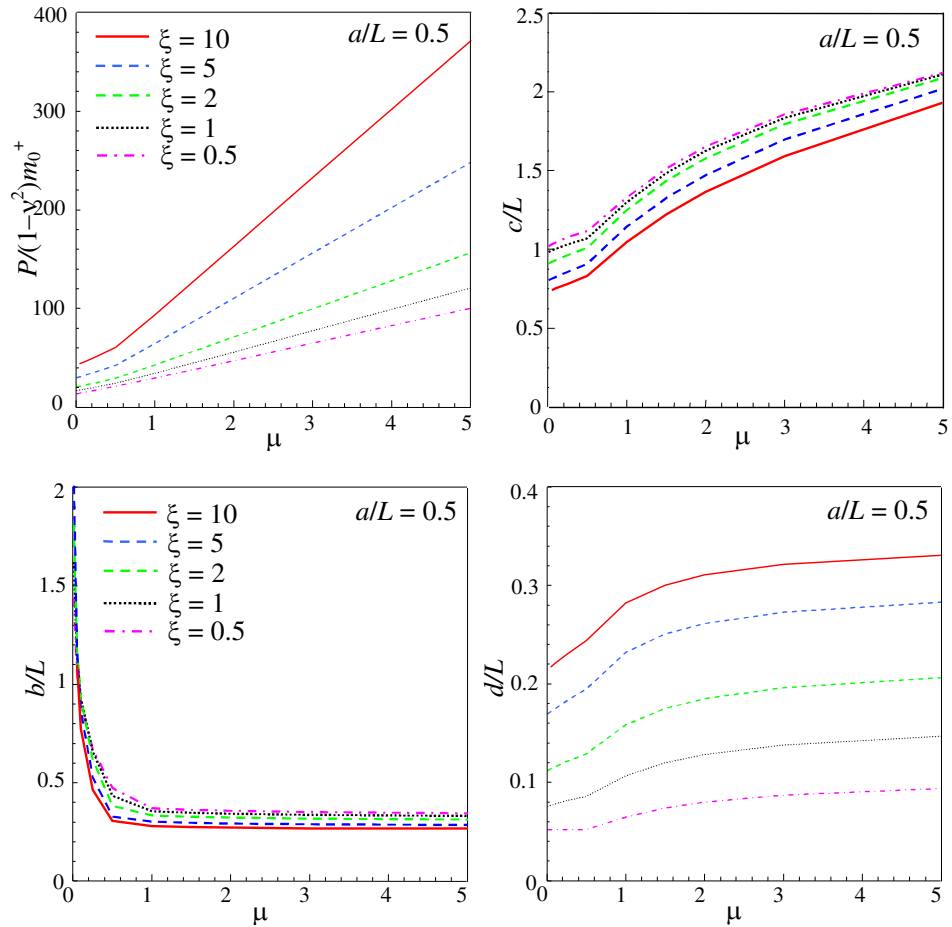


**Figure 11.** Top left: dimensionless ultimate load and dimensionless loci. Top right:  $x/L$ . Bottom left:  $y/L$ . Bottom right:  $d/L$  versus the parameter  $\mu$  for different values of the amplitude  $a$  of the loaded region, for  $\alpha = 0.5$ .

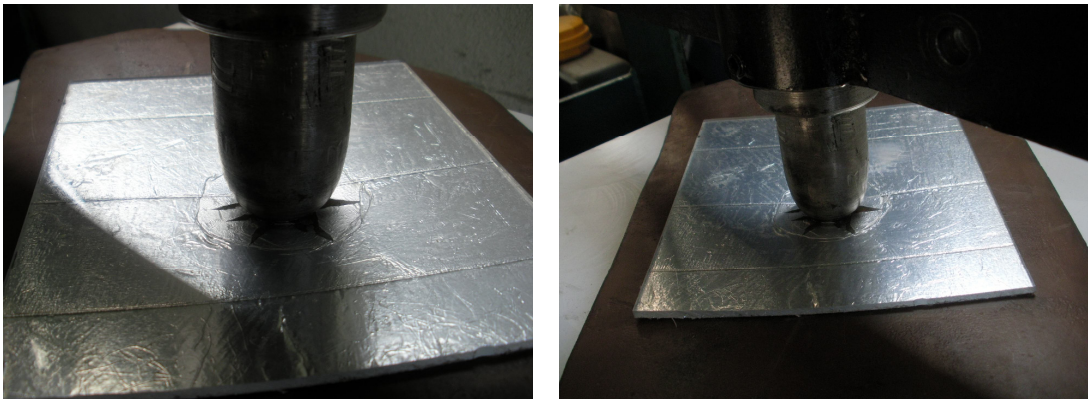


**Figure 12.** Load test on a polycarbonate sheet supported by an elastic support.

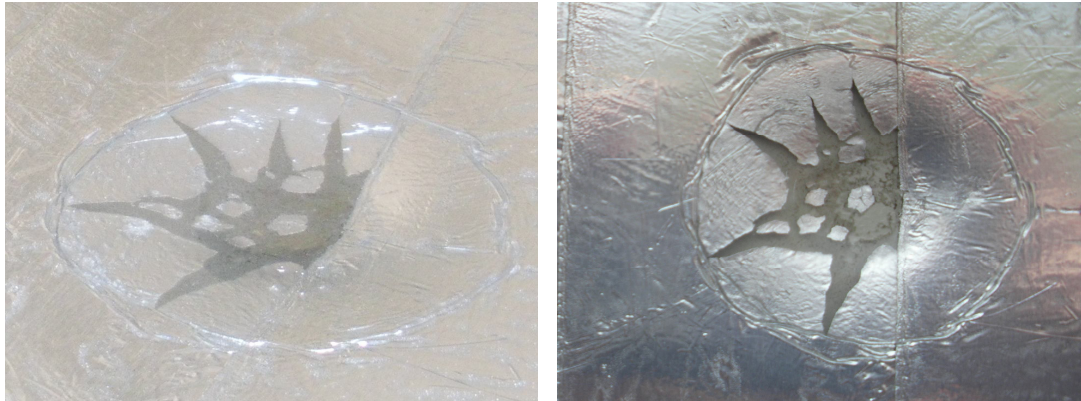


**Figure 13.** Circumferential and radial yield lines in the polycarbonate sheet.

## 6. Conclusions

In this paper, the analysis of an infinite elastic-plastic Kirchhoff plate supported by an elastic two-parameter subgrade has been performed for an arbitrary value of the Pasternak modulus. The elastic-plastic behavior of the plate is assumed to follow Johansen's yield criterion with associative flow rule. A bilateral contact between the paper and the underlying subgrade is assumed, leading to reactive soil pressure which can be compressive as well as tensile.

The analysis shows that the Pasternak modulus  $k_2$  significantly affects through  $\xi$  both the load-carrying capacity of the plate and the size of the elastic-plastic regions at the onset of collapse. However, the effects induced by a variation in the Pasternak modulus are different for small or large amplitudes of the loaded region. For instance, the load-carrying capacity significantly increases as the Pasternak modulus  $k_2$  increases for large sizes  $a/L$  of the loaded region, whereas the increase in the load-carrying capacity is rather moderate for small values of  $a/L$ . Furthermore, an increase in the stiffness of the subgrade in terms of the Pasternak modulus produces a monotonic decrease of the elastic-plastic region of the plate if the loaded region is small, whereas this trend is not monotonic for large amplitudes of the loaded region.

The size of the loaded region  $a/L$  affects the mechanical response of the system also. For large values of the parameter  $a/L$ , an increase in the stiffness parameter  $\xi$  produces indeed an increase of the transverse deflection of the plate; conversely, for moderate values of the parameter  $a/L$ , an increase of the parameter  $\xi$  generates a decrease of the transverse plate deflection. Furthermore, keeping the stiffness of the foundation (i.e., both moduli  $k_1$  and  $k_2$ ) constant, as the size of the load region  $a/L$  increases, the load-carrying capacity of the system increases, as does the amplitude of the elastic-plastic region of the plate.

The effects produced by the ratio  $\mu$  between negative and positive yield moments have been investigated also. It is found that, as  $\mu$  increases, the load-carrying capacity and the radius  $d$  of the fully yielded region  $\theta$  monotonically increase. It is worth noting that the parameter  $\mu$  has a pronounced influence on the load-carrying capacity and amplitude of the annular elastic-plastic regions, but it has almost no effect on the amplitude of the fully plastic inner region  $\theta$  of the plate.

As suggested in Section 5, the model can be applied to assess the mechanical behavior of a plate-like element supported by an elastic medium, providing a prediction of both the load-carrying capacity and plastic mechanism taking place in the elastic-plastic plate.

With the aim of investigating the dynamic behavior of elastic-plastic plates supported by a nonlocal ground, the proposed model can be extended by taking into account also the inertial terms in the equilibrium equations, as in the recent study concerning the dynamical behavior of beams on elastic foundations performed by Piccolroaz and Movchan [2014].

### Acknowledgements

Financial support from “Fondazione Cassa di Risparmio di Modena” within the project “Bando di Ricerca Applicata 2013/2014 — fibra di carbonio e resina IPN” (convention C15414 protocol no. 182.14.8C) is gratefully acknowledged. Lanzoni also gratefully acknowledges support from “Progetto Giovani 2015” by the National Group of Mathematical Physics (GNFM-INdAM).

### References

- [Abramowitz and Stegun 1972] M. Abramowitz and I. A. Stegun (editors), *Handbook of mathematical functions: With formulas, graphs, and mathematical tables*, 10th ed., Wiley, New York, 1972. Reprinted Dover, New York, 1992.
- [Bowles 1997] J. E. Bowles, *Foundation analysis and design*, 5th ed., McGraw-Hill, New York, 1997.
- [Caliendo and Parisi 2010] C. Caliendo and A. Parisi, “Stress-prediction model for airport pavements with jointed concrete slabs”, *J. Transp. Eng. (ASCE)* **136**:7 (2010), 664–677.
- [Çelik and Saygun 1999] M. Çelik and A. Saygun, “A method for the analysis of plates on a two-parameter foundation”, *Int. J. Solids Struct.* **36**:19 (1999), 2891–2915.
- [Duan and Wang 2007] W. H. Duan and C. M. Wang, “Exact solutions for axisymmetric bending of micro/nanoscale circular plates based on nonlocal plate theory”, *Nanotechnology* **18** (2007), 385704.
- [Gazetas 1981a] G. Gazetas, “Ultimate behavior of continuous footings in tensionless contact with a three-parameter soil”, *J. Struct. Mech.* **9**:3 (1981), 339–362.
- [Gazetas 1981b] G. C. Gazetas, “Indentation of anisotropic halfspace by yielding circular foundation”, *J. Eng. Mech. Div. (ASCE)* **107**:4 (1981), 695–704.
- [Gazetas and Tassios 1978] G. C. Gazetas and T. P. Tassios, “Elastic-plastic slabs on elastic foundation”, *J. Struct. Div. (ASCE)* **104**:4 (1978), 621–636.
- [Helwany et al. 1998] S. Helwany, J. Dyer, and J. Leidy, “Finite-element analyses of flexible pavements”, *J. Transp. Eng. (ASCE)* **124**:5 (1998), 491–499.
- [Ince 1944] E. L. Ince, *Ordinary differential equations*, Dover Publications, New York, 1944.
- [Johansen 1962] K. W. Johansen, *Yield-line theory*, Cement and Concrete Association, London, 1962.
- [Kocatürk 1997] T. Kocatürk, “Elastoplastic analysis of circular plates on elastoplastic foundation”, *J. Struct. Eng. (ASCE)* **123**:6 (1997), 808–815.
- [Lanzoni et al. 2014] L. Lanzoni, E. Radi, and A. Nobili, “Ultimate carrying capacity of elastic-plastic plates on a Pasternak foundation”, *J. Appl. Mech. (ASME)* **81**:5 (2014), Article ID 051013.
- [Lewandowski and Świtka 1991] R. Lewandowski and R. Świtka, “Unilateral plate contact with the elastic-plastic Winkler-type foundation”, *Comput. Struct.* **39**:6 (1991), 641–651.
- [Liew et al. 2006] K. M. Liew, X. Q. He, and S. Kitipornchai, “Predicting nanovibration of multi-layered graphene sheets embedded in an elastic matrix”, *Acta Mater.* **54**:16 (2006), 4229–4236.
- [Meyerhof 1960] G. G. Meyerhof, “Bearing capacity of floating ice sheets”, *J. Eng. Mech. Div. (ASCE)* **86**:5 (1960), 113–146.
- [Meyerhof 1962] G. G. Meyerhof, “Load-carrying capacity of concrete pavements”, *J. Soil Mech. Found. Div.* **88**:3 (1962), 89–116.
- [Nobili 2012] A. Nobili, “Variational approach to beams resting on two-parameter tensionless elastic foundations”, *J. Appl. Mech. (ASME)* **79**:2 (2012), 021010.

- [Nobili et al. 2014] A. Nobili, E. Radi, and L. Lanzoni, “A cracked infinite Kirchhoff plate supported by a two-parameter elastic foundation”, *J. Eur. Ceram. Soc.* **34**:11 (2014), 2737–2744.
- [Nobili et al. 2015] A. Nobili, E. Radi, and L. Lanzoni, “On the effect of the backup plate stiffness on the brittle failure of a ceramic armor”, *Acta Mechanica* (online publication August 2015). DOI 10.1007/s00707-015-1412-5.
- [Piccolroaz and Movchan 2014] A. Piccolroaz and A. B. Movchan, “Dispersion and localisation in structured Rayleigh beams”, *Int. J. Solids Struct.* **51**:25–26 (2014), 4452–4461.
- [Pradhan and Kumar 2010] S. C. Pradhan and A. Kumar, “Vibration analysis of orthotropic graphene sheets embedded in Pasternak elastic medium using nonlocal elasticity theory and differential quadrature method”, *Comput. Mater. Sci.* **50**:1 (2010), 239–245.
- [Radi and Di Maida 2014] E. Radi and P. Di Maida, “Analytical solution for ductile and FRC plates on elastic ground loaded on a small circular area”, *J. Mech. Mater. Struct.* **9**:3 (2014), 313–331.
- [Ru 2001] C. Q. Ru, “Axially compressed buckling of a doublewalled carbon nanotube embedded in an elastic medium”, *J. Mech. Phys. Solids* **49**:6 (2001), 1265–1279.
- [Salençon 2013] J. Salençon, *Yield design*, Wiley, Hoboken, NJ, 2013.
- [Save et al. 1997] M. A. Save, C. E. Massonnet, and G. de Saxcé (editors), *Plastic limit analysis of plates, shells and disks*, 2nd ed., North-Holland Series in Applied Mathematics and Mechanics **43**, Elsevier, New York, 1997.
- [Selvadurai 1977] A. P. S. Selvadurai, “Axisymmetric flexure of an infinite plate resting on a finitely deformed incompressible elastic halfspace”, *Int. J. Solids Struct.* **13**:4 (1977), 357–365.
- [Selvadurai 1979] A. P. S. Selvadurai, *Elastic analysis of soil-foundation interaction*, Developments in Geotechnical Engineering **17**, Elsevier, New York, 1979.
- [Shukla et al. 2011] S. K. Shukla, A. Gupta, and N. Sivakugan, “Analysis of circular elastic plate resting on Pasternak foundation by strain energy approach”, *Geotech. Geol. Eng.* **29**:4 (2011), 613–618.
- [Sokół-Supel 1985] J. Sokół-Supel, “Elastoplastic bending of plates resting on elastic subgrade under rotational symmetry conditions”, *J. Struct. Mech.* **13**:3–4 (1985), 323–341.
- [Sokół-Supel 1988] J. Sokół-Supel, “Biegung metallischer Kreisplatten mit elastischer Unterlage”, *Ing. Arch.* **58**:3 (1988), 185–192.
- [Timoshenko and Woinowsky-Krieger 1959] S. Timoshenko and S. Woinowsky-Krieger, *Theory of plates and shells*, 2nd ed., McGraw-Hill, New York, 1959.
- [Tullini et al. 2012] N. Tullini, A. Tralli, and L. Lanzoni, “Intefacial shear stress analysis of bar and thin film bonded to 2D elastic substrate using a coupled FE–BIE method”, *Finite Elem. Anal. Des.* **55** (2012), 42–51.
- [Wen-da and Shu 1987] L. Wen-da and W. Shu, “On the circular footing plates on two-parameters foundation under arbitrary loads”, *Appl. Math. Mech.* **8**:9 (1987), 815–823.

Received 13 Jan 2015. Revised 17 Mar 2015. Accepted 22 Mar 2015.

LUCA LANZONI: [luca.lanzoni@unimo.it](mailto:luca.lanzoni@unimo.it)

DET—Dipartimento di Economia e Tecnologia, Università degli Studi della Repubblica di San Marino, Salita alla Rocca 44, 47890 San Marino città, San Marino and DIEF—Dipartimento di Ingegneria “Enzo Ferrari”, Università di Modena e Reggio Emilia, Via Vignolese 905, I-41125 Modena, Italy

ANDREA NOBILI: [andrea.nobili@unimore.it](mailto:andrea.nobili@unimore.it)

DIEF—Dipartimento di Ingegneria “Enzo Ferrari”, Università di Modena e Reggio Emilia, Via Vignolese 905, I-41125 Modena, Italy

ENRICO RADI: [enrico.radi@unimore.it](mailto:enrico.radi@unimore.it)

DISMI—Dipartimento di Scienze e Metodi dell’Ingegneria, Università di Modena e Reggio Emilia, Via Amendola 2, I-42122 Reggio Emilia, Italy

ANDREA SORZIA: [andrea.sorzia@unimore.it](mailto:andrea.sorzia@unimore.it)

DISMI—Dipartimento di Scienze e Metodi dell’Ingegneria, Università di Modena e Reggio Emilia, Via Amendola 2, I-42122 Reggio Emilia, Italy





# JOURNAL OF MECHANICS OF MATERIALS AND STRUCTURES

[msp.org/jomms](http://msp.org/jomms)

Founded by Charles R. Steele and Marie-Louise Steele

## EDITORIAL BOARD

|                 |   |
|-----------------|---|
| ADAIR R. AGUIAR | University of São Paulo at São Carlos, Brazil   |
| KATIA BERTOLDI  | Harvard University, USA                         |
| DAVIDE BIGONI   | University of Trento, Italy                     |
| YIBIN FU        | Keele University, UK                            |
| IWONA JASIUK    | University of Illinois at Urbana-Champaign, USA |
| C. W. LIM       | City University of Hong Kong                    |
| THOMAS J. PENCE | Michigan State University, USA                  |
| DAVID STEIGMANN | University of California at Berkeley, USA       |

## ADVISORY BOARD

|               |   |
|---------------|---|
| J. P. CARTER  | University of Sydney, Australia                 |
| D. H. HODGES  | Georgia Institute of Technology, USA            |
| J. HUTCHINSON | Harvard University, USA                         |
| D. PAMPLONA   | Universidade Católica do Rio de Janeiro, Brazil |
| M. B. RUBIN   | Technion, Haifa, Israel                         |

**PRODUCTION** [production@msp.org](mailto:production@msp.org)

SILVIO LEVY Scientific Editor

Cover photo: Mando Gomez, [www.mandolux.com](http://www.mandolux.com)

---

See [msp.org/jomms](http://msp.org/jomms) for submission guidelines.


---

JoMMS (ISSN 1559-3959) at Mathematical Sciences Publishers, 798 Evans Hall #6840, c/o University of California, Berkeley, CA 94720-3840, is published in 10 issues a year. The subscription price for 2015 is US\$565/year for the electronic version, and \$725/year (+\$60, if shipping outside the US) for print and electronic. Subscriptions, requests for back issues, and changes of address should be sent to MSP.

---

JoMMS peer-review and production is managed by EditFLOW<sup>®</sup> from Mathematical Sciences Publishers.

PUBLISHED BY

 **mathematical sciences publishers**  
nonprofit scientific publishing

<http://msp.org/>

© 2015 Mathematical Sciences Publishers

# Journal of Mechanics of Materials and Structures

Volume 10, No. 4

July 2015

---

- Relation between the Maxwell equations and boundary conditions in piezoelectric and piezomagnetic fracture mechanics and its application**      HAO TIAN-HU    447
- Axisymmetric loading of an elastic-plastic plate on a general two-parameter foundation**  
LUCA LANZONI, ANDREA NOBILI, ENRICO RADI and ANDREA SORZIA    459
- Contours for planar cracks growing in three dimensions: Illustration for transversely isotropic solid**      LOUIS MILTON BROCK    481
- On Cesàro means of energy in micropolar thermoelastic diffusion theory**  
MARIN MARIN and SAMY REFAHY MAHMOUD    497
- Topology optimization of spatial continuum structures made of nonhomogeneous material of cubic symmetry**  
RADOSŁAW CZUBACKI and TOMASZ LEWIŃSKI    519



1559-3959(2015)10:4;1-9